Cellulose
https://doi.org/10.1007/s10570-026-07047-7

ORIGINAL RESEARCH

Phycocyanin and cellulose nanofibril-based biodegradable triboelectric-piezoelectric hybrid nanogenerators with high-output performance

Ömer Faruk Ünsal · Ebrar Kartal · Ayşe Çelik Bedeloğlu

Received: 22 July 2025 / Accepted: 13 April 2026
© The Author(s) 2026

Abstract In this study, a biodegradable and sustainable piezoelectric–triboelectric hybrid nanogenerator (HENG) was designed and fabricated using cellulose nanofibrils (CNFs) as a nucleating agent and phycocyanin (PC), an algae-derived protein from Spirulina platensis, as the tribo-positive layer paired with poly(vinylidene fluoride) (PVDF) films. The investigation was conducted in two parts to investigate the effect of CNF incorporation into different layers. In the first part, CNFs were incorporated into the PVDF layer, whereas in second part incorporated into the PC layer. Electromechanical performance was characterized under periodic contact–separation motion. Even in the absence of nanofillers, the PVDF–PC pair exhibited efficient electromechanical behavior, generating an open-circuit voltage (V_{oc}) of 84 V and a short-circuit current (I_{sc}) of 87 µA. Upon CNF incorporation, the output was significantly enhanced. The highest performance was observed when CNFs were added to the PVDF layer (at 20 wt.% CNFs loading) with V_{oc} and I_{sc} values of 228 V and 199 µA, respectively. On the other hand, when CNFs were incorporated into the PC layer and paired with neat PVDF, the maximum output reached 128 V and 126 µA (at 5 wt.% CNFs). This outcome highlights that CNFs contribute more effectively to performance improvement in PVDF than in PC.

Keywords Hybrid nanogenerator · Triboelectric · Piezoelectric · Biodegradable nanogenerator · Phycocyanin

Introduction

Nanogenerators (NGs) have attracted considerable attention over the past two decades as energy-harvesting devices, driven by the rise of wireless, wearable, and self-powered electronics. They convert mechanical energy (piezoelectric and triboelectric principles) or thermal energy (pyroelectric effect) into electricity (Yang et al. 2013; Zhang et al. 2015; Alam et al. 2023; Panda et al. 2023). Although their output is lower than that of batteries or solar cells, NGs are well suited for low-power applications such as sensors and lighting (Bharti et al. 2022; Huang and Chung 2025).

Supplementary Information The online version contains supplementary material available at https://doi.org/10.1007/s10570-026-07047-7.

Ö. F. Ünsal (✉) · A. Çelik Bedeloğlu (✉)
Department of Polymer Materials Engineering, Faculty of Engineering and Natural Sciences, Bursa Technical University, Bursa, Turkey
e-mail: omer.unsal@btu.edu.tr

A. Çelik Bedeloğlu
e-mail: ayse.bedeloglu@btu.edu.tr

E. Kartal
Department of Chemical Engineering, Faculty of Engineering, Middle East Technical University, Ankara, Turkey

Published online: 25 April 2026

Triboelectric nanogenerators (TENGs) are the most extensively studied NGs due to their high output voltage and ease of fabrication (Guo et al. 2025; Lou et al. 2025; Lv et al. 2025). In TENGs, current is generated when tribo-positive and tribo-negative materials contact and separate under external mechanical stimuli (Rodrigues-marinho et al. 2020; Wang et al. 2023). Piezoelectric materials are monolithic and homogeneous materials that produce electricity when subjected to external forces such as pressure or bending (Zaarour et al. 2021a). When contact–separation occurs between a piezoelectric and a non-piezoelectric material, both piezoelectric and triboelectric effects contribute, resulting in hybrid nanogenerators (HENGs) (Chen et al. 2019, 2024; Mohamed Yousry et al. 2020; Matin Nazar et al. 2022; Xiao et al. 2024).

In HENGs, although the tribo-layers can be fabricated from polymeric, ceramic, or even metallic materials, polymers are the most commonly used due to their mechanical advantages and allowing broad range of triboelectric properties (Chen et al. 2020; Zhang and Olin 2020; Khandelwal et al. 2021). Recently, a novel, green, and sustainable approach has emerged, that use of bio-based polymers-such as polysaccharides and proteins-as tribo-layers instead of synthetic polymers, in NGs (Meng et al. 2023; Zhu et al. 2024). This strategy not only reduces the carbon footprint of NG devices, but also provides environmental degradation at the end of the device's life cycle (Funayama et al. 2023; Torres et al. 2023; Zhu et al. 2024).

A major challenge in designing bio-based TENGs and HENGs is the intrinsic triboelectric behavior of these materials, as most bio-based polymers exhibit tribo-positive characteristics, limiting strong triboelectric effects (Bai et al. 2020; Nauman et al. 2023; Ghode et al. 2024). Since device performance depends on the polarity difference between tribo-layers, larger disparities yield higher electrical output. A common strategy is to pair a bio-based tribo-positive layer with a strongly tribo-negative synthetic polymer, although this compromises the goal of fully bio-based nanogenerators (Torres et al. 2023). Alternatively, coupling a biopolymer with a piezoelectric polymer enables synergistic energy conversion through both triboelectric and piezoelectric mechanisms (Zhou et al. 2022; Yang et al. 2022; Sarkar et al. 2022).

Poly(vinylidene fluoride) (PVDF) is the most widely used piezoelectric polymer for not only NGs, but also various research areas such as filtration, oil separation, sensors, and actuators (Zaarour et al. 2018, 2020, 2021b, 2022; Correia et al. 2019; Zhang et al. 2022; Meng et al. 2022; Borazan and Celik Bedeloglu 2024; Li et al. 2024a; Zaarour and Mansour 2025). Although some biodegradable polymers (e.g., cellulose, chitosan, poly-L-lactic acid, polyhydroxybutyrate) exhibit piezoelectric effects, PVDF and its derivatives are distinguished by their superior piezoelectric properties. Further, their strongly tribo-negative character also makes them highly suitable for biopolymer-based HENGs (Badatya et al. 2022; Wu et al. 2022; Amrutha et al. 2023; Shee et al. 2024). PVDF-based materials can be processed using a wide range of techniques, including solution-based methods (e.g., electrospinning, solution casting, non-solvent coagulation) and thermoforming methods (e.g., film extrusion, 3D printing, hot pressing). Solution-based techniques are particularly advantageous for nanogenerators, as rapid polymer solidification in processes such as electrospinning or non-solvent coagulation promotes formation of the piezoelectric β-phase (Pickford et al. 2019; He et al. 2021; Song et al. 2022; Frick et al. 2024; Li et al. 2024b). One emerging strategy involves the incorporation of nucleating agents (cellulose nanomaterials, etc.) into the PVDF matrix (Poothanari et al. 2021; Alberts et al. 2021; Zahari et al. 2025).

The use of biopolymers as triboelectric layers in NGs has been reported since 2016 (Chang et al. 2016). While polysaccharides have been widely explored, protein-based films are increasingly favored as tribo-positive layers due to their amide-rich structure and electron-donating behavior, similar to synthetic polyamides (Mahesh et al. 2018; Graham et al. 2022). Keratin and silk fibroin are the most commonly employed proteins in TENG and HENG studies, with silk fibroin-based devices achieving peak voltages up to 2.1 kV and currents of 6.5 μA (Gogurla et al. 2019; Joo et al. 2022; Ram Joshi and Kim 2024; Li et al. 2025; Niu et al. 2025).

However, the use of animal-derived proteins remains controversial due to environmental, economic, and ethical concerns, including high CO_2 emissions, water consumption, waste generation, and animal welfare issues, as well as higher costs and longer production times compared to plant-based proteins (Poore and Nemecek 2018; Langyan et al. 2022; Munialo 2024). Despite these challenges,

plant-derived proteins have been rarely investigated, mainly from grains that are also staple foods (An et al. 2018; Jiang et al. 2022a, b; Bo et al. 2023). In this context, algae-derived materials have emerged as promising candidates for bio-NGs due to their eco-friendly production, short harvesting cycles, and sustainability. Notably, while previous studies on algae-based NGs have focused primarily on polysaccharides as tribo-positive layers, which are slightly tribonegative compared to proteins (Diaz and Felix-Navarro 2004; Pan and Zhang 2019; Zou et al. 2020), the use of algae-derived proteins, such as phycocyanin (PC), remains largely unexplored, presenting an opportunity for the development of novel protein-based bio-NGs (Pang et al. 2018; Torres et al. 2025; Feng et al. 2025). Furthermore, the high protein yield of certain algae species, such as Spirulina platensis, and the relative ease of protein extraction make algae-derived proteins particularly attractive as tribo-positive layers.

In this study, we developed a contact–separation mode HENG with an original design. Device components were 3D-printed from poly(lactic acid) (PLA) via fusion deposition modeling, and tribo-layers were mounted onto the printed parts. The HENG employed PVDF as the tribo-negative layer and the algae-derived polymer PC as the tribo-positive layer, while cellulose nanofibrils (CNFs) were incorporated as nucleating agents for PVDF. To evaluate the synergistic effect of PVDF and CNFs relative to PC-CNF composites, the study was conducted in two parts. In the first, PVDF-CNF films with varying CNF loadings were prepared via non-solvent coagulation and paired with neat PC films in HENGs. In the second, CNFs were incorporated into PC, and PC-CNF films were fabricated via solution casting and paired with coagulated PVDF films. Electromechanical characterization identified the optimal CNF location within the device, and structural analyses by Fourier-transform infrared spectroscopy (FT-IR) and differential scanning calorimetry (DSC) of PVDF, PC, PVDF-CNF, and PC-CNF films supported these findings.

Materials and methods

Materials

PVDF (Alfa Aesar, Germany, MW: 350 kDa), dimethyl formamide (DMF) (ISOLAB Chemicals, Germany), sodium hydroxide (NaOH) (Merck, 99%), sulfuric acid (H_2SO_4) (98%, Merck, Germany), commercial pure cotton (hydrophilic, Lux, Turkey), spirulina algae powder (Algolina, Turkey), and PLA filament (natural, Porima, Turkey) were purchased.

Methods

PC extraction from Spirulina Platensis: The phycocyanin extraction from Spirulina Platensis was performed in three main steps. In the first step, 5 g of algal powder was suspended in 100 mL of deionized water and ultrasonicated at 100 W for 30 min in an ice bath to mechanically disrupt the algal cells. In second step, total volume of solution was increased to 500 mL by adding deionized water, followed by continuous stirring at 300 rpm for 48 h to allow protein diffusion into aqueous phase. In third, the mixture was centrifuged at 9000 rpm for 45 min to provide the separation of insoluble algal residue and PC containing aqueous phase. The supernatant was then concentrated using a rotary evaporator, and the concentrated solution was dried at room temperature to obtain purified phycocyanin.

CNF isolation from cotton: CNF isolation from cotton was conducted according to a previous study with some modifications (Samarawickrama et al. 2023). Initially, 10 g of commercial grade cotton mixed with 200 mL of NaOH solution in a hydrothermal reactor, and delignification process was carried out at 90 °C for 6 h. After 6 h, delignified cotton was washed with deionized water and dried at 40 °C under vacuum. In next step, the cotton was immersed into the 500 mL of 60% sulfuric acid, which had been pre-cooled to 0–5 °C. The mixture was stirred at 500 rpm using a mechanical stirrer for 4 h in an ice bath. Finally, obtained CNF dispersion filtered and washed with deionized water until the pH of filtrate reached between 6 and 7. Purified CNFs were dried at room temperature, in fume hood.

Fabrication of neat and CNF added PC and PVDF films: Polymer films for both layers were fabricated using solution-based methods. Deionized water was used as the solvent for the PC, while PVDF was dissolved in DMF. PC films were prepared by solution casting method. 15 mL of PC solution, which contains 2 wt.% of PC protein, poured into the aluminum weighing dishes with the diameter of 45 mm. Strong adhesion between PC film and aluminum not only

prevented peeling off the PC film from surface, but also allowed the aluminum layer to serve as electrode on PC side. The resulting PC-aluminum layered structures were cut into 15 mm circular shape and directly used as tribo-positive layer in device assembly. On the other hand, PVDF films were obtained by doctor blading and following non-solvent coagulation processes from PVDF solution in DMF (10 wt.%). The polymer solution was casted onto glass surface with the thickness of 250 µm and immersed into the 60 °C water bath to obtain coagulated films. The films were subsequently transferred into a fresh water bath and kept overnight to complete the coagulation after first solidification, followed by drying at room temperature.

Prior to device assembly, one side of each PVDF film was coated 15 mm circular shape with silver via magnetron sputtering to serve as the electrode. CNF addition both for PC and PVDF polymers were carried out by using same procedure. First, appropriate amount of CNFs was added either deionized water (for PC) or DMF (for PVDF) and stirred for 3 h by using a magnetic stirrer. Owing to the strong interactions between CNFs and the respective solvents, uniform dispersions were obtained without the need for ultrasonic homogenization, thereby avoiding potential structural damage to the CNFs. After stirring, corresponding polymer were added into the CNF-solvent dispersion, and CNF-doped polymer solutions were obtained. The film fabrication procedures for CNF-doped samples followed the same protocols as those used for the neat polymer films, as described above.

Device Fabrication: The designed and 3D printed parts were shown in Fig. 1. The parts were fabricated using PLA filament via Creality Ender 3 Pro 3D printer. First, CNF added PC film and/or PVDF film (Fig. 1a) were mounted with a double sided tape onto circular protrusions of different plates (Fig. 1c). Second, two flat shaped springs (Fig. 1b) fixed between two plates and HENG device were obtained (Fig. 1d). Sample codes and required descriptions were given in Table 1.

Characterization: PC and PVDF films were characterized using FT-IR (Nicolet IS50) to verify their molecular and crystalline structures. The analyzed samples included neat PVDF, neat PC, PVDF-CNF20, and PC-CNF5. The effect of CNF incorporation on the crystalline fraction of both films was further examined using DSC (TA DSC25). For DSC analysis, the same set of samples was tested under a

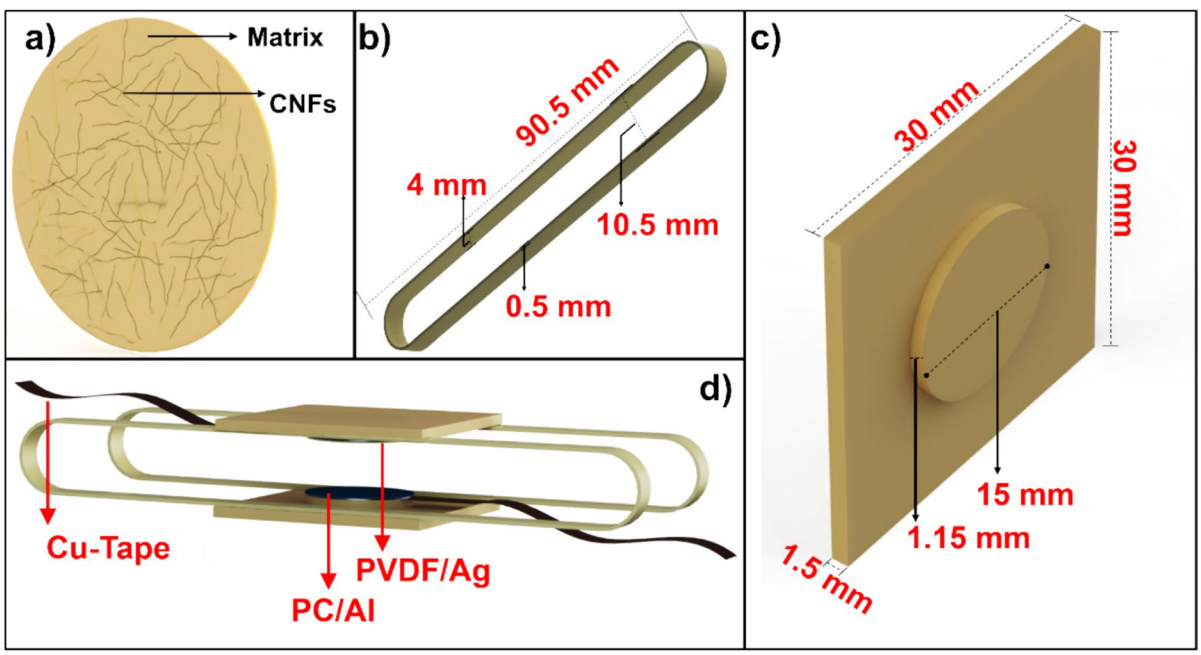


Fig. 1 Schematic illustrations of 3D printed nanogenerator parts; **a** PVDF-CNF or PC-CNF film **b** flat shaped springs, **c** plate, and d resulting nanogenerator device

Table 1 Sample codes and ingredient descriptions

Sample code	Part 1		Part 2	
	PC side	PVDF side	PC side	PVDF side
C1-0	Neat	Neat	–	–
C1-2.5		2.5% CNFs	–	–
C1-5		5% CNFs	–	–
C1-10		10% CNFs	–	–
C1-20		20% CNFs	–	–
C1-30		30% CNFs	–	–
C2-0	–	–	Neat	Neat
C2-1	–	–	1% CNFs	
C2-2	–	–	2% CNFs	
C2-5	–	–	5% CNFs	
C2-10	–	–	10% CNFs	
C2-20	–	–	20% CNFs	

nitrogen atmosphere, with a heating rate of 5 °C/min over the range of 0–240 °C. Morphological investigation for CNFs-added PVDF and PC films was performed with scanning electron microscopy (SEM; Zeiss-Gemini 300), and dimensional measurements were performed on the obtained images with ImageJ software. Finally, electromechanical characterization of HENG devices were performed with a pneumatic periodical compression device (PCD), which has been designed by our research group (Kaplan et al. 2025), under 6 bars of air pressure, and at a frequency of 3.3 Hz. Electromechanical tests were performed in triplicate for each sample. Electrical contacts of HENG devices connected to an oscilloscope (Rigol DS1202Z-E) and output signals were simultaneously acquired under periodic contact-separation motion. Output voltage signals were collected in open-circuit mode, while the HENG contacts were short circuited with a 100kΩ resistor to obtain output current signals.

Results and discussion

SEM images

Figure 2 presents the SEM images of neat and CNFs-added PVDF and PC films. The neat PC film exhibited a relatively smooth surface with a dense internal structure, compared to PVDF based films (Fig. 2a, b). Similar morphological features were observed for the CNF-incorporated PC film (Fig. 2c, d), indicating that the addition of CNFs did not significantly disrupt the surface uniformity or film compactness. Notably, individual CNFs were clearly embedded within the PC matrix, observed both on the film surfaces and within the structural domains. For example, a single CNF bridging two PC blocks (Fig. 2c) serves as direct evidence of homogeneous CNF dispersion within the polymer matrix. On the other hand, SEM images of neat PVDF film (Fig. 2e, f) and PVDF-CNF20 film (Fig. 2g, h) revealed a clear influence of CNF addition on pore structure. CNF addition into the PVDF matrix led to a notable reduction in pore size. Quantitative pore analysis showed that the average pore diameter decreased from 1.43 µm in the neat PVDF film to 0.29 µm in the PVDF-CNF composite film. Additionally, the average diameter of the CNFs embedded in both PC and PVDF matrices was measured as 96.11 nm.

FT-IR results

Figure 1a shows FT-IR spectrums of CNFs, PVDF film and PVDF-CNF film. CNFs have shown characteristic peaks at 3321 cm^{-1} (O–H stretching), 2886 cm^{-1} (C–H stretching), 1427 cm^{-1} (CH_2 scissoring), 1419 cm^{-1} (asymmetrical stretching of C–O–C) 1011 cm^{-1} (C–O–C stretching) (Sahlin et al. 2018; Ogunjobi et al. 2023; Khatun et al. 2023; Duygun and Bedeloğlu 2024; Kaan Duygun and Bedeloğlu 2024) (Figs. 3a, b and S1). On the other hand, FT-IR spectrums of PVDF and PVDF-CNF films showed the interactions between PVDF chains and CNFs. A clear difference between PVDF-CNF and neat PVDF films stands out around 3344 cm^{-1}, which is a characteristic vibration signal of CNFs as mentioned above. However, the wide peak around 3344 cm^{-1} in PVDF-CNF FT-IR spectrum, not only indicates the O–H stretching, but also corresponds to hydrogen bonds between hydroxy groups of CNF and side fluorine atoms of PVDF chain (Figs. 3a and S2) (Boruah et al. 2023; Turossi et al. 2024). Moreover, presence of CNF in PVDF polymer also detected by examining specific α and β crystalline vibration peaks of PVDF chains, due to CNFs are acting as nucleating agent for PVDF. β crystalline phase fraction of a sample can be found via following equation (Li et al. 2013; Faruk Ünsal and Bedeloğlu 2023; Ünsal et al. 2023).

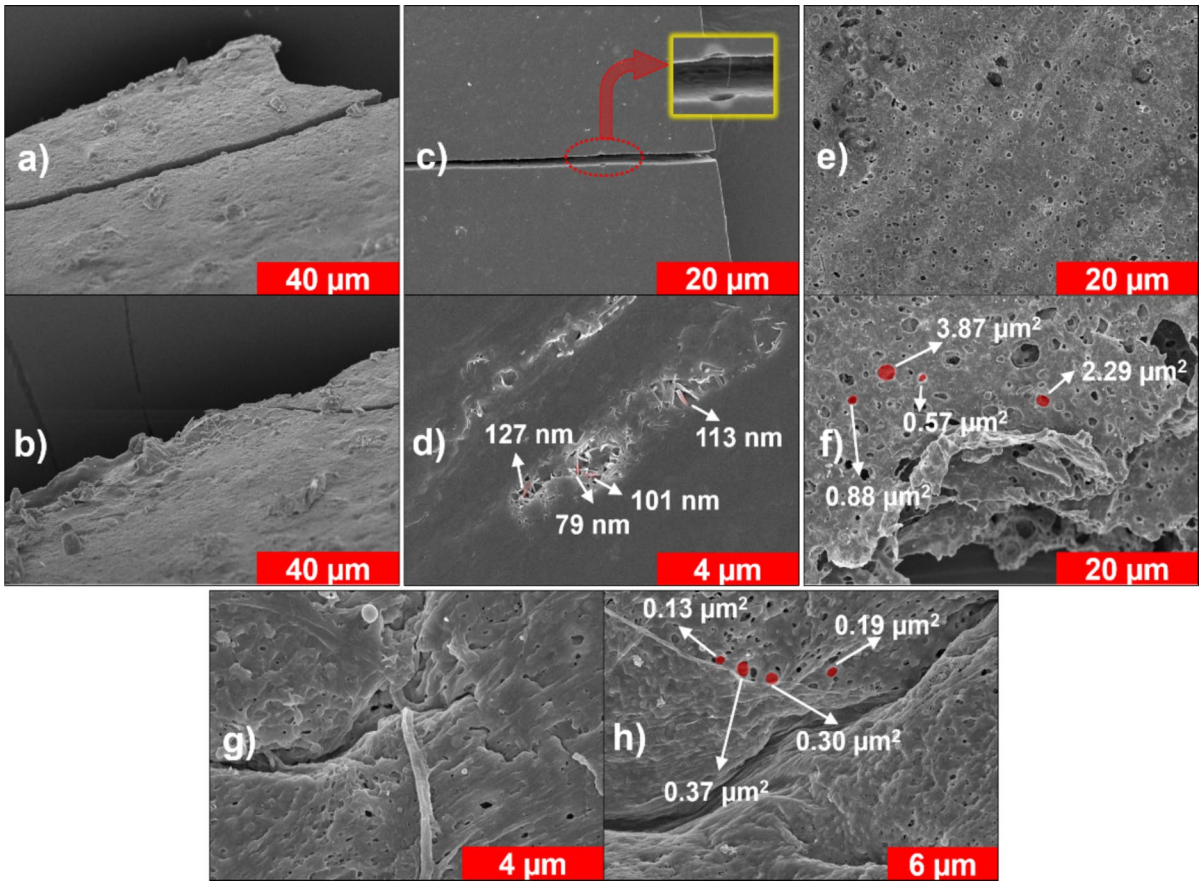


Fig. 2 SEM images of **a** and **b** PC film, **c** and **d** PC-CNF film, **e** and **f** PVDF film, **g** and **h** PVDF-CNF film

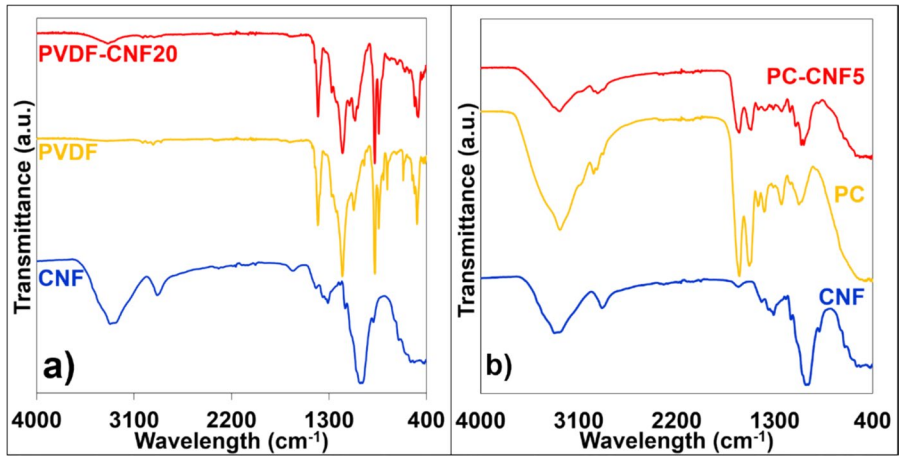


Fig. 3 FT-IR spectrums of **a** CNF, PVDF film and CNF-PVDF film; **b** CNF, PC film, and PC-CNF film

$$F(\beta)\% = \frac{A_\beta}{\left(1.26A_\alpha\right) + A_\beta} \times 100 \quad (1)$$

while the A_α is representing sum of absorption signal intensities of α-crystalline phase peaks, A_β the sum of absorption signal intensities of β-crystalline phase peaks. According to literature, peaks at 613 cm^{-1} and 760 cm^{-1} belong to α-crystalline phase, while the peaks at 509 cm^{-1}, 839 cm^{-1} and 1276 cm^{-1} represents to β-crystalline phase of PVDF macromolecules (Figs. 3b and S2), (Salimi and Yousefi 2003; Li et al. 2013; Gade et al. 2021; Pan et al. 2024). In this regard, the F(β)% of PVDF film and PVDF-CNF film calculated as 64.7% and 77.0%, respectively.

Figure 1b shows FT-IR spectrums of CNFs, PC film and PC-CNF film. Neat PC film showed its characteristic peaks at 3270 cm^{-1} (O–H stretching), 1621 cm^{-1} (C=O stretching from amide I), 1528 cm^{-1} (C=O stretching from amide II), 1449 cm^{-1} and 1391 cm^{-1} (C=N from amide II), 1100 cm^{-1} (C–S stretching from thiocarbonyl bonds) (Figs. 3b and S3) (El-Naggar et al. 2017; Seyed Yagoubi et al. 2018; Prabakaran et al. 2020; Munawaroh et al. 2020; Nair et al. 2023). According to FT-IR curves, cellulose did not play a role more than enhance the IR absorption of film.

DSC results

DSC analysis was performed to evaluate the thermal properties of neat and CNF-loaded PC and PVDF films. Figure 4a shows the DSC thermograms of PVDF and PVDF-CNF films. Both samples exhibited a broad endothermic peak below 50 °C-located at 42.3 °C for neat PVDF and at 47.1 °C for PVDF-CNF. The endothermic peak at 42.3 °C corresponds to the secondary glass transition of the α-crystalline regions of PVDF (Ünsal and Çelik Bedeloğlu 2023). In PVDF-CNF sample, the slightly shifted and broader peak at 47.1 °C is attributed to the combined effects of the secondary glass transition of PVDF and the evaporation of bound water from the CNFs (Udoetok et al. 2018). A sharp endothermic peak, corresponding to the melting of PVDF, was observed at 159.4 °C for neat PVDF and 158.7 °C for the PVDF-CNF composite. The melting enthalpy values were 51.9 J/g and 46.5 J/g for neat and CNF-loaded PVDF films, respectively. The reduction in melting enthalpy in the CNF-loaded sample is attributed to the high loading fraction of CNFs, which may interfere with crystalline packing in the PVDF matrix. The degree of crystallinity for PVDF films was calculated using the following equation (Sun et al. 2010):

$$X_c(\%) = \frac{\Delta H_c}{\varnothing \times \Delta H_c^0} \quad (2)$$

where the ΔH_c is melting enthalpy of sample, $\varnothing$ is the weight fraction of PVDF in composite film, and $\Delta H_c^{\,0}$ is melting enthalpy of 100% crystalline PVDF. The value of $\Delta H_c^{\,0}$ (99.75 °C) was estimated based on the relative proportions of α- and β-crystalline phases, using their known enthalpy values (93.07 J/g and 103.40 J/g, respectively) and phase ratios determined from FTIR analysis. The calculated crystallinity values were 52.0% for neat PVDF and 58.3% for

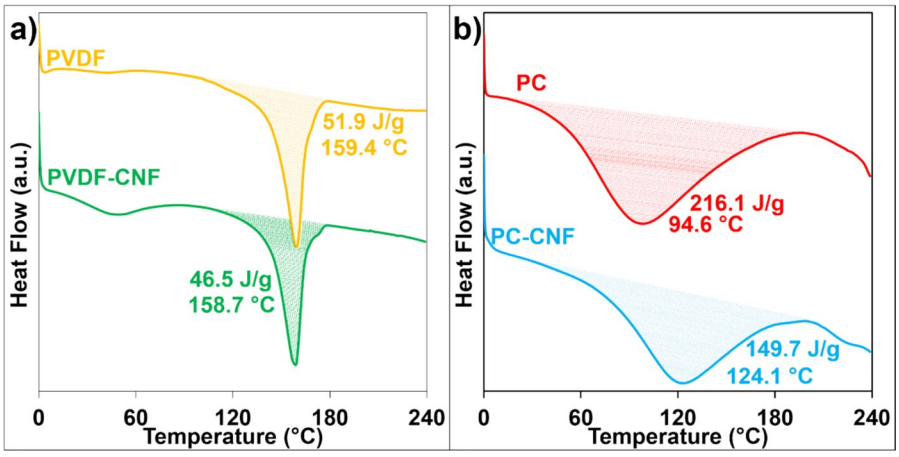


Fig. 4 DSC thermograms of **a** PVDF and PVDF-CNF films and **b** PC and PC-CNF films

PVDF-CNF, indicating a slight enhancement in crystallinity due to CNF incorporation.

Figure 4b presents the DSC thermograms of PC and PC-CNF films. While some of previous studies (Böcker et al. 2020; Lemos et al. 2020; Bai et al. 2024) have attributed the endothermic peak around 94.6 °C to morphological transitions or melting behavior, this peak is more accurately interpreted as the thermal denaturation of protein chains by another part of studies (Mosayebi et al. 2022; Bai et al. 2023). With the addition of CNFs, the denaturation temperature increased significantly from 94.6 °C to 124.1 °C. Furthermore, the denaturation enthalpy decreased from 216.1 J/g (neat PC) to 142.2 J/g for the PC-CNF composite. The increase in denaturation temperature alongside the decrease in enthalpy clearly indicates that CNF incorporation enhances the thermal stability of the PC matrix. These results suggest strong intermolecular interactions between CNFs and PC chains, which restrict the mobility of protein chains and delay thermal degradation.

Electromechanical characterization

Output voltage and current signals of Part 1 and Part 2 were summarized in Fig. 5. In Part 1 (Fig. 5a), it is clearly observed that both the V_{oc} and I_{sc} increased with CNF loading in PVDF films, up to a loading fraction of 20 wt.%. The peak-to-peak V_{oc} rose from 84 V (C1-0) to 228 V for the (C1-20) sample, while the corresponding I_{sc} increased from 84 µA to 199 µA-representing improvements of 171.4% and 128.7%, respectively. However, when CNF content exceeded 20%, both V_{oc} and I_{sc} values declined, dropping to 140 V and 144 µA, respectively for C1-30. This reduction in output signals can be directly attributed to the agglomeration tendency of nanoparticles beyond the percolation threshold in polymer nanocomposites. Agglomerated CNFs are unable to enhance the β-phase fraction in the PVDF polymer, leading to a decreased piezoelectric contribution of the PVDF layer to the HENG device and consequently lower output signals. Additionally, considering the similarity in triboelectric properties between proteins and cellulose, compared to proteins and fluorinated polymers, increasing cellulose fraction in the PVDF layer narrows the triboelectric gap between the PVDF and PC layers, which further reduces the HENG's output performance. In conclusion, the C1-20 HENG device was identified as the optimal configuration in Part 1.

Similar to the Part 1, the incorporation of CNFs into the PC matrix enhanced the output signals in Part 2 (Fig. 5b). The peak-to-peak V_{oc} values were 84 V, 94 V, 96 V, 124 V, 98 V, and 40 V for HENG devices fabricated with PC films containing 0%, 1%, 2%, 5%, 10%, and 20% CNFs, respectively, paired with neat PVDF films. Corresponding I_{sc} values were 87 µA, 97 µA, 116 µA, 128 µA, 126 µA, and 101 µA. Among these, the C2-5 HENG, which consists of 5 wt.% CNF loaded PC film paired with neat PVDF film, exhibited the best performance in Part 2. When comparing the top-performing devices from both parts, C1-20 (PVDF-CNF20) showed superior output performance over C2-5 (PC-CNF5). This result indicates that locating CNF as nucleating agent in PVDF not only promotes enhanced piezoelectric crystalline morphology but also improves triboelectric charge generation yielding higher overall nanogenerator performance.

Further tests were carried out on the optimized C1-20 HENG device. First, the voltage response was recorded under pneumatic pressures ranging from 1 to 8 bar applied by PCD (Fig. 6a). The peak-to-peak V_{oc} remained essentially constant between 152 and 160 V at pressures ≥ 2 bar. However, peak-to-peak V_{oc} was 56 V for 1 bar of applied pressure on PCD. Further, effect of active area on voltage response for C1-20 HENG device also examined. C1-20 HENG devices with the same design in Fig. 1, with a diameter of 15 mm, 20 mm, and 30 mm were fabricated to perform size dependency tests. The output performance of HENG devices with same formulation and various contacting areas was increased with increasing diameter; peak-to-peak V_{oc} for HENG devices were 98 V, 128 V, and 160 V, respectively (Fig. 6b). To evaluate energy-storage capability, the HENG output was rectified (circuit inset, Fig. 6c) and used to charge commercial capacitors of 0.22 µF, 1 µF, 22 µF, and 100 µF. After 60 s of periodic stimuli, the capacitor voltages reached 11.6 V, 10.7 V, 0.64 V, and 0.16 V, respectively, demonstrating efficient charging of low-capacitance devices (Fig. 6c). Moreover, output performance of C1-20 device were also investigated under various resistance loads. The power performance of the C1-20 device was assessed under various external load resistances (Fig. 6d), confirming its suitability for practical energy-harvesting applications. In addition, a stability test were conducted

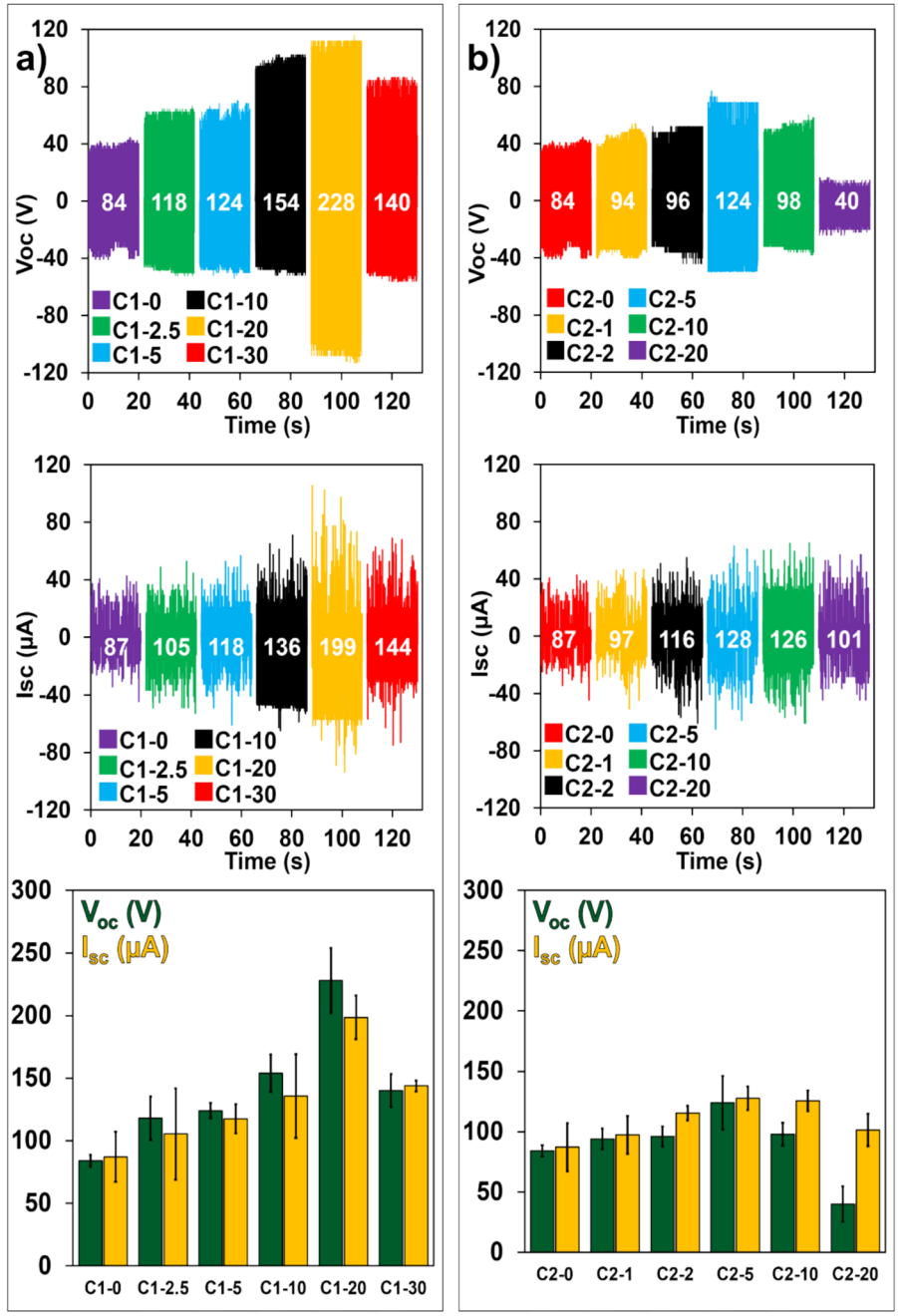


Fig. 5 Voltage and current outputs of HENGs in **a** Part 1 and **b** Part 2

during 6000 cycles (Fig. 6e). Finally, the nanogenerator powered 57 LEDs arranged to display the letters SMR (abbreviation of our research group, SMART MATERIALS RESEARCH), using a rectifier circuit (Fig. 6f).

An extensive literature comparison of protein and algae-derived biopolymer-based TENG and HENG applications is summarized in Table 2. The table clearly shows that particularly the silk fibroin-based tribolayers successfully act as tribopositive layers with high output performance against various tribonegative surfaces. Among these, biodegradable polymers such as poly(lactide-co-glycolide acid) (PLGA) (Xu et al. 2025), and poly(vinyl butyral-co-vinyl alcohol-co-vinyl acetate) (PVBVA) (Ram Joshi and Kim 2024; Joshi and Kim 2024), as well as fluoropolymers

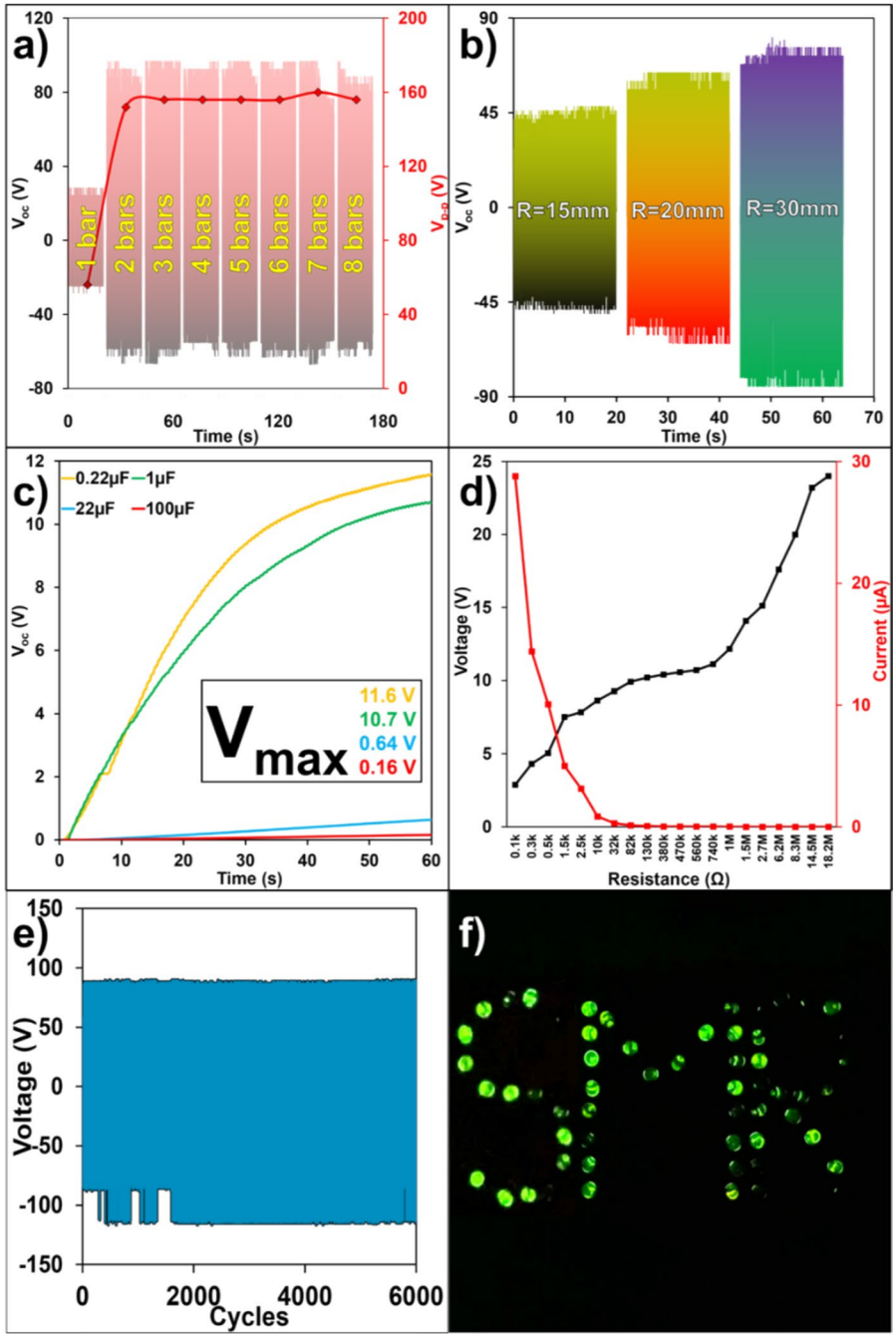


Fig. 6 **a** Voltage response of HENG device under various pressures, **b** active area dependency of HENG device, **c** charging behavior of HENG device on different capacitors, **d** HENG device performance with various resistance loads, **e** stability test result, and **f** nanogenerator-driven lighting of 57 LEDs in "SMR" shape

including fluoro-amides and PTFE (Wang et al. 2024; Niu et al. 2025), stand out as common tribonegative counterparts to silk fibroin. In contrast, studies using other animal-based materials such as chitosan and collagen, enzymes such as lysozyme, or plant-derived polysaccharides such as alginates and Ulvan have generally reported lower output performances against similar tribonegative layers. Notably, PC from Spirulina platensis, when paired with PVDF-a widely used tribonegative polymer for TENGs and HENGs-exhibited impressive performance, achieving a voltage density of 1.29 MV/m^2 and a current density of 1.12 A/m^2. Although the voltage density of the PC/PVDF-based nanogenerator was about 66% lower

Table 2 Protein or algae derived biopolymer based nanogenerator applications

Bio-tribolayer	Voltage density (kV/m^2)	Current density (mA/m^2)	Reference
Silk-fibroin derivate	87.50	7.25	(Xu et al. 2025)
Chitosan	572.40	38.00	(Wu et al. 2025)
Collagen	256.67	9.33	(Zhang et al. 2025)
D-Phenylalanine	53.97	2.97	(Huang et al. 2025)
Silk fibroin	290.00	30.50	(Niu et al. 2025)
Silk fibroin	44.44	-	(Wang et al. 2025)
Silk	653.00	-	(Lee et al. 2025)
Lysozyme	2.06	0.04	(Roy et al. 2025)
Silk fibroin	4222.22	9.78	(Joshi and Kim 2024)
Fibroin and sericin	1862.50	56.25	(Wang et al. 2024)
Silk fibroin	840	2.6	(Ram Joshi and Kim 2024)
Sodium alginate	49	6.6	(Feng et al. 2025)
Calcium alginate/sodium alginate	15.2	0.098	(Pang et al. 2018)
Ulvan	54.8125	2.8125	(Torres et al. 2025)
Phycocyanin	1290.87	1126.68	This Work

than that of silk fibroin-based TENGs (Joshi and Kim 2024), its current density was comparatively high. Based on these findings, it can be inferred that the output performance of PC-based nanogenerators could be further enhanced through material modifications. For example, blending PC with suitable thermoplastic polymers could mitigate its brittleness, thereby improving device durability. Additionally, fabricating the PC layer with a porous morphology-such as a nanofibrous mat, spongy scaffold, or cryogel-could increase the active surface area, promoting more effective triboelectrification in TENG and HENG devices.

Conclusion

A sustainable and highly biodegradable triboelectric-piezoelectric HENG device was successfully designed, fabricated, and characterized using PVDF and PC as active layers, CNF nano-additives, and PLA-based mechanical components. The device output was optimized by not only regulating additive-concentration, but also evaluating the relative contributions of CNFs in the piezoelectric and triboelectric layers. Optimization results clearly demonstrated that CNFs were more effective when incorporated into the piezoelectric PVDF layer, with the optimal performance observed at a 20 wt.% CNF loading. The PVDF-CNF20/PC-based HENG exhibited V_{oc} and I_{sc} values that were 2.7 and 2.3 times higher, respectively, than those of the neat PVDF/PC-based device. This enhancement is attributed to the CNF-induced increase in the β-phase content of PVDF. FTIR-based calculations showed that the β-crystalline phase fraction increased from 64.7% (neat PVDF) to 77.0% upon CNF incorporation. Although CNF addition to the PC layer also improved output performance, the effect was attractive as the first part, reinforcing the conclusion that CNFs are more effective in enhancing piezoelectric behavior than triboelectric charge generation. Nonetheless, DSC analysis revealed that CNF incorporation also improved the thermal stability of the PC protein. This improvement suggests that CNFs can expand the application potential of algae-derived PC beyond energy harvesting to areas such as biomedical devices, green textiles, food science, and sustainable materials development.

Author contributions Ömer Faruk ÜNSAL: conceptualization, materials fabrication and characterization, writing, visualization, data analysis and processing. Ebrar KARTAL: materials fabrication and characterization. Ayşe ÇELİK BEDELOĞLU: conceptualization and writing.

Funding Open access funding provided by the Scientific and Technological Research Council of Türkiye (TÜBİTAK). This study has not been funded by any organization.

Data availability Data is provided within the manuscript or supplementary information files.

Declarations

Conflict of interest The authors declare no competing interests.

Ethical approval Not applicable.

Open Access This article is licensed under a Creative Commons Attribution 4.0 International License, which permits use, sharing, adaptation, distribution and reproduction in any medium or format, as long as you give appropriate credit to the original author(s) and the source, provide a link to the Creative Commons licence, and indicate if changes were made. The images or other third party material in this article are included in the article's Creative Commons licence, unless indicated otherwise in a credit line to the material. If material is not included in the article's Creative Commons licence and your intended use is not permitted by statutory regulation or exceeds the permitted use, you will need to obtain permission directly from the copyright holder. To view a copy of this licence, visit http://creativecommons.org/licenses/by/4.0/.

References

Alam SN, Ghosh A, Shrivastava P et al (2023) An introduction to triboelectric nanogenerators. Nano-Struct Nano-Objects 34:100980. https://doi.org/10.1016/J.NANOSO.2023.100980

Alberts EM, Peel HR, Warner CM, et al (2021) Synthesis and characterization of biological nanomaterial/poly(vinylidene fluoride) composites. https://doi.org/10.21079/11681/42132

Amrutha B, Prasad G, Sathiyanathan P et al (2023) Fabrication of CuO-NP-doped PVDF composites based electrospun triboelectric nanogenerators for wearable and biomedical applications. Polymers (Basel) 15:2442. https://doi.org/10.3390/POLYM15112442/S1

An S, Sankaran A, Yarin AL (2018) Natural biopolymer-based triboelectric nanogenerators via fast, facile, scalable solution blowing. ACS Appl Mater Interfaces 10:37749–37759. https://doi.org/10.1021/ACSAMI.8B15597/SUPPL_FILE/AM8B15597_SI_003.AVI

Badatya S, Bhowal R, Mandal K et al (2022) Poling-polarization-mediated centrosymmetric charge-transfer organic-cocrystal-based flexible triboelectric nanogenerator. ACS Appl Electron Mater 4:3665–3678. https://doi.org/10.1021/ACSAELM.2C00630/SUPPL_FILE/EL2C00630_SI_003.MP4

Bai Z, Xu Y, Zhang Z et al (2020) Highly flexible, porous electroactive biocomposite as attractive tribopositive material for advancing high-performance triboelectric nanogenerator. Nano Energy 75:104884. https://doi.org/10.1016/J.NANOEN.2020.104884

Bai Y, Li X, Xie Y et al (2023) Ultrasound treatment enhanced the functional properties of phycocyanin with phlorotannin from Ascophyllum nodosum. Front Nutr 10:1181262. https://doi.org/10.3389/FNUT.2023.1181262/BIBTEX

Bai Y, Wang Y, Li X et al (2024) Interaction mechanism and binding mode of phycocyanin to lysozyme: molecular docking and molecular dynamics simulation. Food Chem 438:138001. https://doi.org/10.1016/J.FOODCHEM.2023.138001

Bharti DK, Veeralingam S, Badhulika S (2022) An ultra high performance, lead-free Bi2WO6:P(VDF-TrFE)-based triboelectric nanogenerator for self-powered sensors and smart electronic applications. Mater Horiz 9:663–674. https://doi.org/10.1039/D1MH01606G

Bo X, Uyanga KA, Wang L et al (2023) High power-output and highly stretchable protein-based biomechanical energy harvester. Chem Eng J 451:138714. https://doi.org/10.1016/J.CEJ.2022.138714

Böcker L, Hostettler T, Diener M et al (2020) Time-temperature-resolved functional and structural changes of phycocyanin extracted from *Arthrospira platensis*/*Spirulina*. Food Chem 316:126374. https://doi.org/10.1016/J.FOODCHEM.2020.126374

Borazan İ, Celik Bedeloglu A (2024) Self-standing piezoelectric nanogenerator fabrics from ZnO-doped PVDF nanofiber yarns. J Appl Polym Sci 141:e54948. https://doi.org/10.1002/APP.54948

Boruah P, Gupta R, Katiyar V (2023) Fabrication of cellulose nanocrystal (CNC) from waste paper for developing antifouling and high-performance polyvinylidene fluoride (PVDF) membrane for water purification. Carbohydr Polym Technol Appl 5:100309. https://doi.org/10.1016/J.CARPTA.2023.100309

Chang TH, Peng YW, Chen CH et al (2016) Protein-based contact electrification and its uses for mechanical energy harvesting and humidity detecting. Nano Energy 21:238–246. https://doi.org/10.1016/J.NANOEN.2016.01.017

Chen CY, Tsai CY, Xu MH et al (2019) A fully encapsulated piezoelectric-triboelectric hybrid nanogenerator for energy harvesting from biomechanical and environmental sources. Express Polym Lett 13:533–542. https://doi.org/10.3144/expresspolymlett.2019.45

Chen A, Zhang C, Zhu G et al (2020) Polymer materials for high-performance triboelectric nanogenerators. Adv Sci 7:2000186. https://doi.org/10.1002/ADVS.202000186

Chen Q, Cao Y, Lu Y et al (2024) Hybrid piezoelectric/triboelectric wearable nanogenerator based on stretchable PVDF-PDMS composite films. ACS Appl Mater Interfaces 16:6239–6249. https://doi.org/10.1021/ACSAMI.3C15760/SUPPL_FILE/AM3C15760_SI_003.MP4

Correia DM, Barbosa JC, Costa CM et al (2019) Ionic liquid cation size-dependent electromechanical response of ionic liquid/poly(vinylidene fluoride)-based soft actuators. J Phys Chem C 123:12744–12752. https://doi.org/10.1021/ACS.JPCC.9B00868/SUPPL_FILE/JP9B00868_SI_001.AVI

Diaz AF, Felix-Navarro RM (2004) A semi-quantitative triboelectric series for polymeric materials: the influence of

chemical structure and properties. J Electrostat 62:277–290. https://doi.org/10.1016/J.ELSTAT.2004.05.005

Duygun İK, Bedeloğlu A (2024) Ti3C2Tx MXene/reduced graphene oxide/cellulose nanocrystal-coated cotton fabric electrodes for supercapacitor applications. J Mater Sci 59:9455–9471. https://doi.org/10.1007/s10853-024-09784-1

El-Naggar NEA, Hussein MH, El-Sawah AA (2017) Bio-fabrication of silver nanoparticles by phycocyanin, characterization, in vitro anticancer activity against breast cancer cell line and in vivo cytotxicity. Sci Rep 7(1):1–20. https://doi.org/10.1038/s41598-017-11121-3

Faruk Ünsal Ö, Bedeloğlu AÇ, elīk, (2023) Three-dimensional piezoelectric-triboelectric hybrid nanogenerators for mechanical energy harvesting. ACS Appl Nano Mater. https://doi.org/10.1021/acsanm.3c01973

Feng Q, Xie Z, Wen Y et al (2025) An eco-friendly, sodium alginate degradable conformal triboelectric nanogenerator for self-powered sensing and real-time injury monitoring. Sustain Mater Technol 43:e01262. https://doi.org/10.1016/J.SUSMAT.2025.E01262

Frick A, van Vliet WA, Žukauskaitė A et al (2024) Volumetric 3D-printed piezoelectric polymer films. Adv Mater Technol 9:2301469. https://doi.org/10.1002/ADMT.202301469

Funayama R, Hayashi S, Terakawa M (2023) Fabrication of biodegradable triboelectric nanogenerator by laser-induced graphitization of lignin/PLLA composite sheets. Laser Appl Microelectron Optoelectron Manuf (LAMOM) 12408:19–24. https://doi.org/10.1117/12.2646915

Gade H, Nikam S, Chase GG, Reneker DH (2021) Effect of electrospinning conditions on β-phase and surface charge potential of PVDF fibers. Polymer (Guildf) 228:123902. https://doi.org/10.1016/J.POLYMER.2021.123902

Ghode SB, Patil OA, Chougale MY et al (2024) *Terminalia chebula* fruits powder as tribopositive material for high-performance triboelectric nanogenerator. Energy Technol 12:2300984. https://doi.org/10.1002/ENTE.202300984

Gogurla N, Roy B, Park JY, Kim S (2019) Skin-contact actuated single-electrode protein triboelectric nanogenerator and strain sensor for biomechanical energy harvesting and motion sensing. Nano Energy 62:674–681. https://doi.org/10.1016/J.NANOEN.2019.05.082

Graham SA, Patnam H, Manchi P et al (2022) Superficial modification of polyamide-66 film for enhanced electrical performance and multimode functional triboelectric nanogenerators. Int J Energy Res 46:17391–17403. https://doi.org/10.1002/ER.8405

Guo R, Luo H, He S et al (2025) Performance metrics of triboelectric nanogenerator toward record-high output energy density. Energy Environ Sci. https://doi.org/10.1039/D5EE00376H

He Z, Rault F, Lewandowski M et al (2021) Electrospun PVDF nanofibers for piezoelectric applications: a review of the ınfluence of electrospinning parameters on the β phase and crystallinity enhancement. Polym 13:174. https://doi.org/10.3390/POLYM13020174

Huang YJ, Chung CK (2025) Research on performance enhancement, output regulation, and the applications of nanogenerators. Micromachines 16(2):208. https://doi.org/10.3390/MI16020208

Huang J, Xia J, Baddi S et al (2025) Dual-scale polarization engineering of d-Phenylalanine-based assemblies for high-performance nanogenerators. ACS Nano. https://doi.org/10.1021/ACSNANO.5C03436/SUPPL_FILE/NN5C03436_SI_003.MP4

Jiang C, He C, Lin R et al (2022a) Engineering squandered plant protein into eco-friendly triboelectric films for highly efficient energy harvesting. Nano Energy 101:107589. https://doi.org/10.1016/J.NANOEN.2022.107589

Jiang C, Zhang Q, He C et al (2022b) Plant-protein-enabled biodegradable triboelectric nanogenerator for sustainable agriculture. Fundam Res 2:974–984. https://doi.org/10.1016/J.FMRE.2021.09.010

Joo S, Kim JH, Lee CE et al (2022) Eco-friendly keratin-based additives in the polymer matrix to enhance the output of triboelectric nanogenerators. ACS Appl Bio Mater 5:5706–5715. https://doi.org/10.1021/ACSABM.2C00736/SUPPL_FILE/MT2C00736_SI_004.MP4

Joshi SR, Kim S (2024) Functional silk-protein-based nanocomposites for light-stimulated and highly efficient triboelectric nanogenerators and charge storage devices. J Power Sources 624:235538. https://doi.org/10.1016/J.JPOWSOUR.2024.235538

Kaan Duygun İ, Bedeloğlu A (2024) MXene/cellulose nanocrystal-coated cotton fabric electrodes for wearable electronics. Appl Nanosci 14(3):575–584. https://doi.org/10.1007/S13204-024-03034-1

Kaplan M, Alp E, Borazan İ et al (2025) Enhanced piezoelectric performance of poly(vinylidene fluoride) nanocomposites with synthesized zinc oxide nanowires and branched carbon nanotubes via melt mixing process. Macromol Mater Eng. https://doi.org/10.1002/mame.202500122

Khandelwal G, Prashanth N, Raj MJ et al (2021) Materials beyond conventional triboelectric series for fabrication and applications of triboelectric nanogenerators. Adv Energy Mater 11:2101170. https://doi.org/10.1002/AENM.202101170

Khatun MA, Sultana S, Islam Z et al (2023) Extraction of crystalline nanocellulose (CNC) from date palm mat fibers and its application in the production of nanocomposites with polyvinyl alcohol and polyvinylpyrrolidone blended films. Results Eng 17:101031. https://doi.org/10.1016/J.RINENG.2023.101031

Langyan S, Yadava P, Khan FN et al (2022) Sustaining protein nutrition through plant-based foods. Front Nutr 8:772573. https://doi.org/10.3389/FNUT.2021.772573/XML

Lee S, Son W, Joshi SR et al (2025) μm-thick and water-taping protein electronic tattoos for multifunctional on-skin electronics. Small. https://doi.org/10.1002/SMLL.202503580

Lemos PVF, Opretzka LCF, Almeida LS et al (2020) Preparation and characterization of C-phycocyanin coated with STMP/STPP cross-linked starches from different botanical sources. Int J Biol Macromol 159:739–750. https://doi.org/10.1016/J.IJBIOMAC.2020.05.111

Li L, Zhang M, Rong M, Ruan W (2013) Studies on the transformation process of PVDF from α to β phase by stretching. RSC Adv 4:3938–3943. https://doi.org/10.1039/C3RA45134H

Li W, Xie A, Jiang J et al (2024a) Fabrication and application of flexible piezoelectric sensor based on electrospun PVDF-TrFE nanofibers. J Phys: Conf Ser 2740:012029. https://doi.org/10.1088/1742-6596/2740/1/012029

Li X, Yuan CX, Gao G et al (2024b) All-organic shell–core PVDF/PMMA composite fiber films with enhanced piezoelectric performance for flexible sensing and energy harvesting. J Appl Polym Sci 141:e55626. https://doi.org/10.1002/APP.55626

Li M, Jiang T, Liu S et al (2025) A high output wool felt-based double-ring triboelectric nanogenerator with durability and humidity resistance for ocean navigation. Nano Energy 135:110654. https://doi.org/10.1016/J.NANOEN.2025.110654

Lou Y, Li M, Yu A et al (2025) An ultra-high output self-managed power system based on a multilayer magnetic suspension hybrid nanogenerator for harvesting water wave energy. Energy Environ Sci 18:1745–1755. https://doi.org/10.1039/D4EE04205K

Lv H, Wang Z, Gao Z, Song H (2025) Highly stretchable, self-healable, and environment-adaptable ionogel-based high-output triboelectric nanogenerator for self-powered wearable ionotronics. Chem Eng J 509:161247. https://doi.org/10.1016/J.CEJ.2025.161247

Mahesh S, Tang KC, Raj M (2018) Amide bond activation of biological molecules. Mol 23:2615. https://doi.org/10.3390/MOLECULES23102615

Matin Nazar A, Egbe KJI, Jiao P (2022) Hybrid piezoelectric and triboelectric nanogenerators for energy harvesting and walking sensing. Energ Technol 10:2200063. https://doi.org/10.1002/ENTE.202200063

Meng X, Li Q, Hu Z, Guo M (2022) Microfluidic fabrication of β-phase enriched poly(vinylidene fluoride) microfibers toward flexible piezoelectric sensor. J Polym Sci 60:1718–1726. https://doi.org/10.1002/POL.20210952

Meng H, Yu Q, Liu Z et al (2023) Triboelectric performances of biodegradable polymers. Matter 6:4274–4290. https://doi.org/10.1016/J.MATT.2023.09.017

Mohamed Yousry Y, Yao K, Mahmoud Mohamed A et al (2020) Theoretical model and outstanding performance from constructive piezoelectric and triboelectric mechanism in electrospun PVDF fiber film. Adv Funct Mater 30:1910592. https://doi.org/10.1002/ADFM.201910592

Mosayebi V, Fathi M, Shahedi M et al (2022) Fast-dissolving antioxidant nanofibers based on Spirulina protein concentrate and gelatin developed using needleless electrospinning. Food Biosci 47:101759. https://doi.org/10.1016/J.FBIO.2022.101759

Munawaroh HSH, Gumilar GG, Alifia CR et al (2020) Photostabilization of phycocyanin from *Spirulina platensis* modified by formaldehyde. Process Biochem 94:297–304. https://doi.org/10.1016/J.PROCBIO.2020.04.021

Munialo CD (2024) A review of alternative plant protein sources, their extraction, functional characterisation, application, nutritional value and pinch points to being the solution to sustainable food production. Int J Food Sci Technol 59:462–472. https://doi.org/10.1111/IJFS.16467

Nair MS, Rajarathinam R, Velmurugan S et al (2023) Phycocyanin-conjugated chitosan-coated iron oxide nanoparticles for the separation of Escherichia coli cells. Biomass Convers Biorefinery. https://doi.org/10.1007/S13399-023-04529-7/FIGURES/10

Nauman A, Ameen S, Kim HR (2023) Antibiotic-powered energy harvesting: ıntroducing benzylpenicillin as an efficient tribopositive material for triboelectric nanogenerators. Nanomater 13:2995. https://doi.org/10.3390/NANO13232995

Niu Q, Shen J, Liang W et al (2025) Fully biodegradable ion-induced silk fibroin-based triboelectric nanogenerators with enhanced performance prevent muscle atrophy. Biomaterials 318:123185. https://doi.org/10.1016/J.BIOMATERIALS.2025.123185

Ogunjobi JK, Adewale AI, Adeyemi SA (2023) Cellulose nanocrystals from Siam weed: synthesis and physicochemical characterization. Heliyon 9:e13104. https://doi.org/10.1016/J.HELIYON.2023.E13104

Pan S, Zhang Z (2019) Fundamental theories and basic principles of triboelectric effect: a review. Friction 7:2–17. https://doi.org/10.1007/S40544-018-0217-7/METRICS

Pan L, Wang Y, Jin Q et al (2024) Self-poled PVDF/recycled cellulose composite fibers utilizing cellulose nanocrystals to induce PVDF β-phase formation through wet-spinning as a flexible fabric piezoelectric sensor. Chem Eng J 479:147742. https://doi.org/10.1016/J.CEJ.2023.147742

Panda S, Hajra S, Song H et al (2023) Pyroelectric based energy harvesting devices: hybrid structures and applications. Sustain Energy Fuels 7:5319–5335. https://doi.org/10.1039/D3SE01180A

Pang Y, Xi F, Luo J et al (2018) An alginate film-based degradable triboelectric nanogenerator. RSC Adv 8:6719–6726. https://doi.org/10.1039/C7RA13294H

Pickford T, Gu X, Heeley EL, Wan C (2019) Effects of an ionic liquid and processing conditions on the β-polymorph crystal formation in poly(vinylidene fluoride). CrystEngComm 21:5418–5428. https://doi.org/10.1039/C9CE01051C

Poore J, Nemecek T (2018) Reducing food's environmental impacts through producers and consumers. Science 360:987–992. https://doi.org/10.1126/SCIENCE.AAQ0216/SUPPL_FILE/AAQ0216_DATAS2.XLS

Poothanari MA, Michaud V, Damjanovic D, Leterrier Y (2021) Surface modified microfibrillated cellulose-poly(vinylidene fluoride) composites: β-phase formation, viscoelastic and dielectric performance. Polym Int 70:1316–1328. https://doi.org/10.1002/PI.6202

Prabakaran G, Sampathkumar P, Kavisri M, Moovendhan M (2020) Extraction and characterization of phycocyanin from *Spirulina platensis* and evaluation of its anticancer, antidiabetic and antiinflammatory effect. Int J Biol Macromol 153:256–263. https://doi.org/10.1016/J.IJBIOMAC.2020.03.009

Ram Joshi S, Kim S (2024) High power triboelectric nanogenerator based on nanofibers of silk protein and PVBVA and its motion sensing applications. Chem

Eng J 489:151248. https://doi.org/10.1016/J.CEJ.2024.151248

Rodrigues-marinho T, Castro N, Correia V et al (2020) Triboelectric energy harvesting response of different polymer-based materials. Mater 13:4980. https://doi.org/10.3390/MA13214980

Roy K, Mallick Z, O'Mahony C et al (2025) Engineered lysozyme: an eco-friendly bio-mechanical energy harvester. Energy Environ Mater 8:e12787. https://doi.org/10.1002/EEM2.12787

Sahlin K, Forsgren L, Moberg T et al (2018) Surface treatment of cellulose nanocrystals (CNC): effects on dispersion rheology. Cellulose 25:331–345. https://doi.org/10.1007/S10570-017-1582-5/FIGURES/7

Salimi A, Yousefi AA (2003) Analysis method: FTIR studies of β-phase crystal formation in stretched PVDF films. Polym Test 22:699–704. https://doi.org/10.1016/S0142-9418(03)00003-5

Samarawickrama KGR, Wijayapala UGS, Fernando CAN (2023) Extraction and analysis of cellulose nanocrystals from cotton balls by acid hydrolysis. J Sci Univ Kelaniya 16:23–29. https://doi.org/10.4038/JOSUK.V16I1.8075

Sarkar L, Kandala AB, Bonam S et al (2022) Flexible polymer-based triboelectric nanogenerator using Poly(vinylidene fluoride) and *Bombyx mori* silk. Mater Today Sustain 20:100230. https://doi.org/10.1016/J.MTSUST.2022.100230

Seyed Yagoubi A, Shahidi F, Mohebbi M et al (2018) Preparation, characterization and evaluation of physicochemical properties of phycocyanin-loaded solid lipid nanoparticles and nanostructured lipid carriers. J Food Meas Charact 12:378–385. https://doi.org/10.1007/S11694-017-9650-Y/FIGURES/8

Shee C, Banerjee S, Bairagi S et al (2024) A critical review on polyvinylidene fluoride (PVDF)/zinc oxide (ZnO)-based piezoelectric and triboelectric nanogenerators. J Phys Energy 6:032001. https://doi.org/10.1088/2515-7655/AD405B

Song H, Song W, Song JH et al (2022) Electrospun 1D and 2D Carbon and polyvinylidene fluoride (PVDF) piezoelectric nanocomposites. J Nanomater 2022:9452318. https://doi.org/10.1155/2022/9452318

Sun LL, Li B, Zhang ZG, Zhong WH (2010) Achieving very high fraction of β-crystal PVDF and PVDF/CNF composites and their effect on AC conductivity and microstructure through a stretching process. Eur Polym J 46:2112–2119. https://doi.org/10.1016/J.EURPOLYMJ.2010.09.003

Torres FG, Gonzales KN, Troncoso OP et al (2023) A review on the development of biopolymer nanocomposite-based triboelectric nanogenerators (bio-TENGs). ACS Appl Electron Mater 5:3546–3559. https://doi.org/10.1021/ACSAELM.3C00621/ASSET/IMAGES/MEDIUM/EL3C00621_0004.GIF

Torres FG, Troncoso OP, Cornejo G, Tapia J (2025) Triboelectric nanogenerators based on Ulvan biopolymer: impact of Lithium sulfate doping on electrical output. Energy Technol. https://doi.org/10.1002/ENTE.202500310

Turossi TC, Duarte J, Zattera AJ, Baldasso C (2024) Fabrication of anti-fouling membranes of polyvinylidene fluoride (PVDF) with the addition of cellulose nanofibers (CNF). Desalin Water Treat 318:100379. https://doi.org/10.1016/J.DWT.2024.100379

Udoetok IA, Wilson LD, Headley JV (2018) Ultra-sonication assisted cross-linking of cellulose polymers. Ultrason Sonochem 42:567–576. https://doi.org/10.1016/J.ULTSONCH.2017.12.017

Ünsal ÖF, Çelik Bedeloğlu A (2023) Nanofiber mat-based highly compact piezoelectric-triboelectric hybrid nanogenerators. Express Polym Lett 17:564–579

Ünsal ÖF, Altın Y, Çelik Bedeloğlu A (2023) Flexible electrospun PVDF piezoelectric nanogenerators with electrospray-deposited graphene electrodes. J Electron Mater 52:2053–2061. https://doi.org/10.1007/s11664-022-10169-w

Wang H, Huang S, Kuang H et al (2023) A united triboelectrification mechanism for contacts between all types of materials. Adv Energy Mater 13:2300529. https://doi.org/10.1002/AENM.202300529

Wang Q, Xu B, Tan D et al (2024) Nature-inspired scalable high-performance triboelectric nanogenerators for energy harvesting and sensing. Nano Energy 121:109217. https://doi.org/10.1016/J.NANOEN.2023.109217

Wang M, Lu S, Liu Y, Liu Y (2025) Half-side deposited TiO2 on silk fibroin films: for thermal comfort wearable triboelectric nanogenerators. Chem Eng J 505:159120. https://doi.org/10.1016/J.CEJ.2024.159120

Wu Q, Yu Z, Huang F, Gu J (2022) Electrospun PA66/graphene fiber films and application on flexible triboelectric nanogenerators. Mater 15:5191. https://doi.org/10.3390/MA15155191

Wu P, Liu Y, Wang F et al (2025) Magnetically driven wireless implantable interface polarization-enhanced triboelectric nanogenerator for promoting neural cell differentiation. Nano Energy 136:110703. https://doi.org/10.1016/J.NANOEN.2025.110703

Xiao Y, Wang Y, Yang L et al (2024) A high-performance flexible arch-shaped tribo-piezoelectric hybrid nanogenerator for energy harvesting. Energy Technol 12:2300770. https://doi.org/10.1002/ENTE.202300770

Xu C, Long Y, Feng L et al (2025) Bionic triboelectric nanogenerator activates the "mechano-electro-biochemical" cascade effect in situ to accelerate critical-sized bone defect repair. Adv Mater. https://doi.org/10.1002/ADMA.202504128

Yang Y, Zhang H, Zhu G et al (2013) Flexible hybrid energy cell for simultaneously harvesting thermal, mechanical, and solar energies. ACS Nano 7:785–790. https://doi.org/10.1021/NN305247X/SUPPL_FILE/NN305247X_SI_002.AVI

Yang M, Tian X, Hua T (2022) Green and recyclable cellulose based TENG for sustainable energy and human-machine interactive system. Chem Eng J 442:136150. https://doi.org/10.1016/J.CEJ.2022.136150

Zaarour B, Mansour G (2025) Fabrication of perfect branched PVDF/TiO2 nanofibers for keeping food fresh via one-step electrospinning. NANO. https://doi.org/10.1142/S1793292025500183

Zaarour B, Zhu L, Huang C, Jin X (2018) Fabrication of a polyvinylidene fluoride cactus-like nanofiber through one-step electrospinning. RSC Adv 8:42353–42360. https://doi.org/10.1039/C8RA09257E

Zaarour B, Zhu L, Jin X (2020) Direct generation of electrospun branched nanofibers for energy harvesting. Polym Adv Technol 31:2659–2666. https://doi.org/10.1002/PAT.4992

Zaarour B, Zhu L, Huang C et al (2021a) A review on piezoelectric fibers and nanowires for energy harvesting. J Ind Text 51:297–340. https://doi.org/10.1177/1528083719870197/ASSET/A12FB45B-4976-43BB-BBB1-7D8DAB633F8F/ASSETS/IMAGES/LARGE/10.1177_1528083719870197-FIG22.JPG

Zaarour B, Zhu L, Jin X (2021b) Direct fabrication of electrospun branched nanofibers with tiny diameters for oil absorption. J Dispers Sci Technol 42:2085–2091. https://doi.org/10.1080/01932691.2020.1798779

Zaarour B, Tina H, Zhu L, Jin XY (2022) Branched nanofibers with tiny diameters for air filtration via one-step electrospinning. J Ind Text 51:1105S-1117S. https://doi.org/10.1177/1528083720923773/SUPPL_FILE/SJ-PDF-1-JIT-10.1177_1528083720923773.PDF

Zahari AS, Mazwir MH, Misnon II et al (2025) Piezoelectric and dielectric properties of electrospun Polyvinylidene Fluoride (PVDF) blended with Cellulose Nanocrystals (CNCs). Macromol Symp 414:2300248. https://doi.org/10.1002/MASY.202300248

Zhang R, Olin H (2020) Material choices for triboelectric nanogenerators: a critical review. EcoMat 2:e12062. https://doi.org/10.1002/EOM2.12062

Zhang H, Zhang S, Yao G et al (2015) Simultaneously harvesting thermal and mechanical energies based on flexible hybrid nanogenerator for self-powered cathodic protection. ACS Appl Mater Interfaces 7:28142–28147. https://doi.org/10.1021/ACSAMI.5B10923/SUPPL_FILE/AM5B10923_SI_002.AVI

Zhang C, Yu H, Sun H, Zhu Q (2022) Property enhancement in flexible poly(vinylidene fluoride)-based piezoelectric films with large-area preparation. J Appl Polym Sci 139:51698. https://doi.org/10.1002/APP.51698

Zhang W, Li W, Yan M et al (2025) Power generation from leather scrap waste: fabrication and application of a novel self-morphologized collagen fiber-based triboelectric nanogenerator. Chem Eng J 510:161801. https://doi.org/10.1016/J.CEJ.2025.161801

Zhou J, Wang H, Du C et al (2022) Cellulose for sustainable triboelectric nanogenerators. Adv Energy Sustain Res 3:2100161. https://doi.org/10.1002/AESR.202100161

Zhu Q, Sun E, Zhao Z et al (2024) Biopolymer materials in triboelectric nanogenerators: a review. Polymers 16:1304. https://doi.org/10.3390/POLYM16101304

Zou H, Guo L, Xue H et al (2020) Quantifying and understanding the triboelectric series of inorganic non-metallic materials. Nat Commun 11:1–7. https://doi.org/10.1038/s41467-020-15926-1

Publisher's Note Springer Nature remains neutral with regard to jurisdictional claims in published maps and institutional affiliations.